

# A variational framework for fiber-reinforced viscoelastic soft tissues including damage

J. M. Vassoler<sup>1</sup>, L. Stainier<sup>2</sup> and E. A. Fancello<sup>3,\*</sup>,<sup>†</sup>

<sup>1</sup>*Department of Mechanical Engineering, Universidade Federal do Rio Grande do Sul, Porto Alegre, RS, Brazil*

<sup>2</sup>*Institute of Civil and Mechanical Engineering, Ecole Centrale de Nantes, Nantes, France*

<sup>3</sup>*Department of Mechanical Engineering, Universidade Federal de Santa Catarina, Florianópolis, SC, Brazil*

## SUMMARY

Fibrous soft biological tissues such as skin, ligaments, tendons, and arteries are non-homogeneous composite materials composed of fibers embedded in a ground substance. Cyclic tensile tests on these type of materials usually show a hysteretic stress–strain behavior in which strain rate dependence (viscoelasticity) and softening (Mullins' effect) play a coupled role. The main contribution of the present paper is to present unified variational approach to model both coupled phenomena: nonlinear viscoelasticity and Mullins-like softening behavior. The approach is labeled as variational because viscous-strain and damage internal variables are updated based on the minimization of a hyperelastic-like potential that takes a renewed value at each time step. Numerical examples explores (a) the versatility of the proposed model to account for the two described phenomena according to the chosen functions for the free-energy and dissipative potentials, (b) the ability of the time-integration scheme embedded in the incremental potential definition to allow for large time increments, and (c) the capability of the model to mimic experimentally obtained stress–strain cyclic curves of soft tissues. The model implementation on standard finite elements is also tested in which symmetric analytic tangent matrices are used as a natural consequence of the variational nature of the proposed approach. Copyright © 2016 John Wiley & Sons, Ltd.

Received 27 December 2014; Revised 8 February 2016; Accepted 9 February 2016

KEY WORDS: mechanical damage; viscoelasticity; anisotropy; biological tissues

## 1. INTRODUCTION

Fibrous soft biological tissues such as skin, ligaments, tendons, and arteries are non-homogeneous composite materials composed of fibers embedded in a ground substance or matrix. Fibers are mainly composed of elastin – long flexible molecules forming three-dimensional networks by cross-linking – and collagen, the main structural component of the tissue. The particular arrangement of the collagen proteins – three left-handed helices twisted together into a right-handed triple helix – provides this structure with a high stretch resistance to traction. The collagen molecules group to form collagen fibrils, and bundles of these fibrils cluster into collagen fibers. These fibers are organized in networks whose structure differs depending on the tissue functional requirements. Tendons and ligaments have a pronounced parallel arrangement; arteries and skin are organized in biaxial layers of fibers, while triaxial structures are found, for example, in cartilages. The matrix or ground substance is mostly composed of extracellular material with high content of water, which provides high resistance to volume variations as well as viscous mechanical properties [1, 2].

\*Correspondence to: E. A. Fancello, Department of Mechanical Engineering, Universidade Federal de Santa Catarina, Campus Universitário, Trindade, 88040-900, Florianópolis, SC, Brazil.

<sup>†</sup>E-mail: fancello@grante.ufsc.br

The main observed macroscopic mechanical behaviors of these materials are

- Anisotropy, as a consequence of the composite structural arrangement;
- High nonlinear strain–stress relationship;
- Strain rate dependence, due to solid/fluid and fiber/matrix interactions;
- Dependency on preconditioning and on the last maximum strain level previously achieved, phenomenon commonly referred as Mullins' effect [3];
- Damage, when stretched beyond physiological thresholds; and
- Permanent strains, related with the previous two items.

A nonlinear anisotropic model applied to fibrous connective tissues is early addressed in [1] where the concept of a strain energy function, based on the addition of the strain energy of each tissue's component is used. In [4], a model is presented for transversely isotropic soft tissues, based on the work of Spencer [5], using invariants related to the Cauchy–Green deformation tensor and the fiber directions, concept that is widely used in recent models. In [6], a polyconvex framework for transversely isotropic soft tissues is proposed, later used in the simulation of atherosclerotic arteries [7].

Pioneer works of Simo [8] and Govindjee and Simo [9] proposed models that addressed viscoelasticity and damage and strongly influenced further developments.

In [10], the authors highlight these works and proposes a Kelvin–Voigt-type viscoelastic model for ligaments following the approach defined by Holzapfel and Gasser [11]. Later, in [12], the importance of the viscoelasticity phenomenon in ligaments is enhanced, pointing out the need of nonlinear viscoelastic models in order to adequately reproduce this time dependence.

Damage, preconditioning, and Mullins' effect are all interrelated. This last phenomenon, originally devised in filled rubbers, received significant attention, and many models attempt for its proper representation [13, 14]. In [15], the model incorporates a scalar damage variable to the transversely anisotropic part of the strain energy, assuming that damage in arterial walls occurs mainly in the fiber directions. In [16–18], the authors follow the approach of Simo [8] in which, based on the concept of a yield surface, damage is completely determined by the maximum attained strain level, using the square root of the undamaged strain energy (equivalent strain) as an intermediate variable. In [19, 20], the authors considered a statistical approach related to length distribution of collagen fibers to define damage on the anisotropic part of the strain energy, while a deterministic damage variable accounts for the softening in the isotropic counterpart. In [21], is proposed a model in which internal variables control softening in predefined directions of an anisotropic material. Mullins' effect is achieved as a particular case of a preconditioning process.

The physiological evidence of permanent deformation for highly strained tissues induced models to consider this phenomenon [21–24].

Based on the theoretical background proposed in [25] and [26], a viscoelastic framework for finite strain nonlinear viscoelastic materials was proposed in [27], later used in [28]. The same nonlinear viscoelastic background was recently considered in [29] where anisotropy due to fiber reinforcement was addressed.

The objective of this paper is to introduce a set of damage-like internal variables within the previous variational anisotropic nonlinear viscoelastic framework [29] and therefore being capable of reproducing typical softening behavior like Mullins' effect coupled with nonlinear viscoelasticity. In this unified approach, damage evolution (issue that in [8, 16–18] is accounted by using a damage yield criterion) naturally arises as the result of a constrained minimization problem. Moreover, tangent matrices remain symmetric and available by analytic expressions. Despite the declared application aims at the simulation of biological fibered soft tissues, the model is flexible enough to accommodate other fiber reinforced viscoelastic-damaging materials.

In Section 2, the mathematical background of the variational framework is presented. Section 3 describes the theoretical contribution of this paper, i.e., the introduction of coupled viscoelastic-damage behavior within a unified variational basis. In this section, particular attention is deserved to a consistent time-integration scheme for the incremental potential definition to allow for large time increments. Section 4 shows examples designed to explore (a) the versatility of the proposed model to account for the two described phenomena according to the chosen functions for the free-energy

and dissipative potentials, (b) the ability of the time-integration scheme embedded in the incremental potential definition to allow for large time increments, and (c) the capability of the model to mimic experimentally obtained stress–strain cyclic curves of soft tissues. The model implementation on standard finite elements is also tested in which symmetric analytic tangent matrices are used as a natural consequence of the variational nature of the proposed approach. Final remarks and conclusions are shown in Section 5.

## 2. VARIATIONAL CONSTITUTIVE APPROACH

Classical hyperelastic models are based on the existence of a free energy function  $\Psi$  dependent only on the gradient of deformation  $\mathbf{F}$  or, because of material objectivity, to the Cauchy–Green tensor  $\mathbf{C} = \mathbf{F}^T \mathbf{F}$ . The first Piola–Kirchhoff stress tensor  $\mathbf{P}$  is obtained as the derivative of  $\Psi$  with respect to  $\mathbf{F}$  or  $\mathbf{C}$ :

$$\mathbf{P} = \frac{\partial \Psi(\mathbf{F})}{\partial \mathbf{F}} = 2\mathbf{F} \frac{\partial \Psi(\mathbf{C})}{\partial \mathbf{C}} \tag{1}$$

Assuming the satisfaction of compatibility and constitutive equations, the problem of equilibrium may be defined as the minimization of the potential energy defined over the undeformed configuration  $\Omega_0$  with boundary  $\Gamma_0$ :

$$\begin{aligned} \mathbf{x}^* &= \arg \min_{\mathbf{x} \in \mathcal{K}} \mathcal{H}(\mathbf{x}) \\ \mathcal{H}(\mathbf{x}) &= \int_{\Omega_0} \Psi(\mathbf{F}(\mathbf{x})) d\Omega_0 - \left[ \int_{\Omega_0} \mathbf{b}_0 \cdot \mathbf{x} d\Omega_0 + \int_{\Gamma_0} \mathbf{f}_0 \cdot \mathbf{x} d\Gamma_0 \right] \end{aligned} \tag{2}$$

where  $\mathbf{b}_0$  and  $\mathbf{f}_0$  are the body and surface forces on the reference configuration and  $\mathcal{K}$  the set of admissible deformations. Necessary optimality conditions lead to the known principle of virtual work

$$\int_{\Omega_0} \mathbf{P}(\mathbf{F}(\mathbf{x})) : \nabla \delta \mathbf{x} d\Omega_0 - \left[ \int_{\Omega_0} \mathbf{b}_0 \cdot \delta \mathbf{x} d\Omega_0 + \int_{\Gamma_0} \mathbf{f}_0 \cdot \delta \mathbf{x} d\Gamma_0 \right] = 0 \quad \forall \delta \mathbf{x} \in \mathcal{V} \tag{3}$$

being  $\mathcal{V}$  the set of virtual deformations.

Differently from the previous hyperelastic case, stress in dissipative materials depends not only on the total deformation but also on its history, which, in the context of continuum thermodynamics, can be taken into account by a set of internal state variables. In [25] and [26], a variational approach is proposed in which an incremental potential  $\Psi$  is defined at each time step and the first Piola–Kirchhoff can be computed analogously to (1) as follows:

$$\mathbf{P}_{n+1} = \frac{\partial \Psi(\mathbf{F}_{n+1}; \xi_n)}{\partial \mathbf{F}_{n+1}} = 2\mathbf{F}_{n+1} \frac{\partial \Psi(\mathbf{C}_{n+1}; \xi_n)}{\partial \mathbf{C}_{n+1}} \tag{4}$$

The set  $\xi = \{\mathbf{F}, \mathbf{F}^i, \mathbf{Q}\}$  includes all external and internal state variables, while subscripts  $n$  and  $n + 1$  indicate the incremental positions in time. Depending on the specific model, the gradient of deformation may be decomposed multiplicatively ( $\mathbf{F} = \mathbf{F}^e \mathbf{F}^i$ ), providing elastic and inelastic gradients of deformation. The latter is an internal state variable associated with the state variable  $\mathbf{F}$ . The symbol  $\mathbf{Q}$  includes all remaining internal variables related to the dissipative phenomena. In [25], it is shown that the incremental potential may have the generic expression as a function of the free energy  $W$  and a dissipation pseudo-potential  $\psi$ :

$$\Psi(\mathbf{F}_{n+1}; \xi_n) = \min_{\mathbf{F}_{n+1}^i, \mathbf{Q}_{n+1}} \left\{ W(\xi_{n+1}) - W(\xi_n) + \Delta t \psi \left( \dot{\mathbf{F}}^i, \dot{\mathbf{Q}}; \xi_{n+\alpha} \right) \right\} \tag{5}$$

Potential  $\psi$  provides the necessary information for the evolution of the internal variables and is capable to introduce the dependence of the stress on the rates  $\dot{\mathbf{F}}^i$  and  $\dot{\mathbf{Q}}$ . The subscripts  $n + \alpha$  represents an intermediate time position between  $n$  and  $n + 1$ .

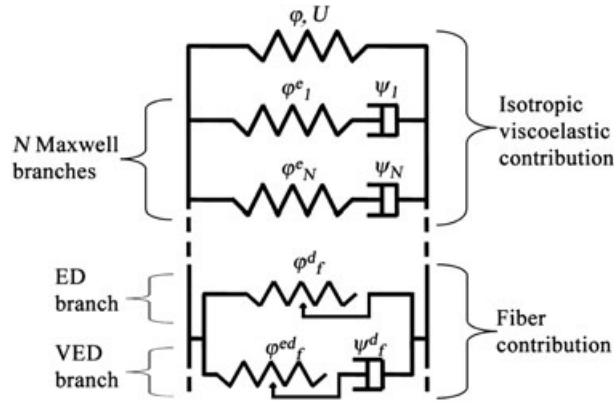


Figure 1. Rheological model.

The minimization problem (5) identifies the optimal values of  $\mathbf{F}_{n+1}^i$  and  $\mathbf{Q}_{n+1}$ , and consequently the internal variables update associated with the new state  $\mathbf{F}_{n+1}$ . Once this update is performed, the stress tensor  $\mathbf{P}_{n+1}$  is computed using expression (4).

### 3. ANISOTROPIC VISCOELASTIC DAMAGE MODEL

The model proposed here is an extension of that presented in [29] making it capable to represent two important phenomena: the so-called Mullins' effect and softening at large strains. The Mullins' effect is frequently reported in filled polymers, where a loss of stiffness at strain levels below the maximum previously attained can be observed. The second one is related to the breakage of collagen fibers at excessive high strains. Both behaviors are treated here by including damage-type internal variables.

Following a common approach for anisotropic reinforced materials [4, 5, 30], we use here an additive decomposition of the incremental potential into isotropic and fiber-reinforced anisotropic contributions<sup>‡</sup>:

$$\Psi = \Psi_{iso} + \Psi_f \tag{6}$$

The potential  $\Psi_{iso}$  was proposed in [27] and accounts for the isotropic response of the material. The contribution of  $\Psi_f$  was set up in [29] and represents the directional (anisotropic) behavior of the fibers. Figure 1 shows a rheological representation of the addition (6) in which both, the isotropic and the fiber contributions, are connected in parallel reacting independently of each other for the same total strain.

In the present work, potential  $\Psi_f$  is modified to accommodate two damage-type internal variables. This is discussed in detail in the next items.

#### 3.1. Isotropic viscoelastic incremental potential

As already mentioned, the potential  $\Psi_{iso}$  used in this work is exactly that proposed in [27] and mimics the rheological representation of Figure 1. The gradient of deformation is decoupled into isochoric and volumetric parts  $\hat{\mathbf{F}} = \mathbf{F}J^{-1}$ ,  $J = \det(\mathbf{F})$ , while the isochoric tensor  $\hat{\mathbf{F}}$  is also multiplicatively decoupled into elastic and viscous contributions:  $\hat{\mathbf{F}} = \hat{\mathbf{F}}^e \mathbf{F}^v$ . Multiplicative decomposition of strains applied to viscoelastic constitutive equations goes back to the work of Sidoroff [31] and later to [32, 33]. The free energy  $W$  of (5) is then split in three terms:

<sup>‡</sup>The classical additive decomposition in Equation (6) implies that both isotropic and anisotropic contributions are uncoupled. From the point of view of composite modeling, this approach represents the simplest composite approximation based on mixture rules.

$$W = \varphi(\hat{\mathbf{C}}) + U(J) + \varphi^e(\hat{\mathbf{C}}^e), \quad \hat{\mathbf{C}} = \hat{\mathbf{F}}^T \hat{\mathbf{F}}, \quad \hat{\mathbf{C}}^e = \hat{\mathbf{F}}^{eT} \hat{\mathbf{F}}^e \tag{7}$$

Potentials  $\varphi$  and  $U$ , associated with the first branch of Figure 1, account for the elastic strain energy accumulated because of the total isochoric and volumetric quantities  $\hat{\mathbf{C}}$  and  $J$ , respectively. Similarly,  $\varphi^e$  represents the elastic strain energy accumulated in the second branch of Figure 1, because of the isocoric deformation tensor  $\hat{\mathbf{C}}^e$ .

The dissipative potential  $\psi$  of (5) depends on the viscous stretching  $\mathbf{D}^v$

$$\psi = \psi(\mathbf{D}^v), \quad \mathbf{D}^v = \text{Sym}(\mathbf{L}^v) = \mathbf{L}^v = \dot{\mathbf{F}}^v \mathbf{F}^{v-1} \tag{8}$$

which it is conveniently expressed in terms of spectral decomposition. At time  $t_{n+1}$ , we have  $\mathbf{D}_{n+1}^v = \sum_{j=1}^3 \frac{\Delta q_j}{\Delta t} \mathbf{M}_j$ , where  $\Delta q_j / \Delta t$  and  $\mathbf{M}_j$  are the eigenvalues and eigenprojections of  $\mathbf{D}_{n+1}^v$ . Substituting all these assumptions in (5) yields the following (local) minimization problem:

$$\Psi_{iso}(\mathbf{F}_{n+1}; \xi_n) = \Delta\varphi(\hat{\mathbf{C}}_{n+1}) + \Delta U(J_{n+1}) + \min_{\mathbf{M}_j, \Delta q_j} \left\{ \Delta\varphi^e(\hat{\mathbf{C}}_{n+1}^e) + \Delta t \psi(\mathbf{D}_{n+1}^v) \right\} \tag{9}$$

subject to a set of constraints that keep the viscous stretching isochoric:

$$\Delta q_j \in K_Q = \{p_j \in \mathbb{R} \Rightarrow p_1 + p_2 + p_3 = 0\} \tag{10}$$

$$\mathbf{M}_j \in K_M = \{\mathbf{N}_j \in \text{Sym} \Rightarrow \mathbf{N}_j \cdot \mathbf{N}_j = 1, \mathbf{N}_i \cdot \mathbf{N}_j = 0, i \neq j\} \tag{11}$$

In expression (9), we used the notation

$$\Delta[\cdot](\cdot)_{n+1} = [\cdot](\cdot)_{n+1} - [\cdot](\cdot)_n$$

It is proven in [27, 34] that the minimization of (9) with respect to  $\mathbf{M}_j$  can be solved analytically leading to the convenient results that  $\mathbf{M}_j = \mathbf{E}_j^{pr}$ ,  $j = 1, 2, 3$ , where  $c_j^{pr}$ ,  $\mathbf{E}_j^{pr}$  are the eigenvalues and eigenprojections of the (predictor) deformation tensor  $\hat{\mathbf{C}}^{pr} = (\hat{\mathbf{F}}^{pr})^T \hat{\mathbf{F}}^{pr}$ ,  $\hat{\mathbf{F}}^{pr} = \hat{\mathbf{F}}_{n+1} \mathbf{F}_n^{v-1}$ .

Finally, the minimization with respect to  $\Delta q_j^v$  drives to a system of four nonlinear optimality conditions. If Newton method is chosen to solve it, the solution provides the symmetric analytical tangent modulus needed for the global equilibrium problem. Details of the model and all mathematical corresponding operations are found in [27].

### 3.2. Anisotropic viscoelastic damage incremental potential

Potential  $\Psi_f$  follows the same structure proposed in [29] and can be schematically represented in the second part of Figure 1. Because of the anisotropic contribution of fibers, it depends not only on the Cauchy tensor  $\mathbf{C}$  but also on the material structural tensor  $\mathbf{A}_f = \mathbf{a}_f \otimes \mathbf{a}_f$ , where  $\mathbf{a}_f$  is the unit vector on the fiber direction of the undeformed configuration. This dependence in the present case is related to the invariant  $I_f$ :

$$I_f = \text{tr}[\hat{\mathbf{C}}\mathbf{A}_f] = \hat{\mathbf{C}} : \mathbf{A}_f = \mathbf{a}_f \cdot \hat{\mathbf{C}}\mathbf{a}_f = \lambda_f^2 \tag{12}$$

and has the particular physical meaning of the isochoric quadratic stretch  $\lambda_f^2$  in the direction of the fiber. Other possible invariants were here avoided to keep the model as simple as possible and also to avoid the difficulties associated with material parameter identification. It should be noted that the choice of  $\hat{\mathbf{C}}$  to define  $I_f$ , already adopted by other authors [11], may lead to non-physical responses in the case of compressibility [35]. However, in this proposal, the volumetric potential in (8) should be understood as a penalty term to enforce the incompressibility condition commonly assumed in biological tissues.

The first branch (ED) of the fiber contribution in Figure 1 is then dependent on the total stretch  $\lambda_f$  in the fiber direction. The second branch (VED) involves the decomposition of the total elongation  $\lambda_f$  into elastic and viscous contributions  $\lambda_f = \lambda_f^e \lambda_f^v$ . The logarithmic strains related to the elongation and viscous stretching are defined as

$$\varepsilon_f = \ln \lambda_f, \quad \varepsilon_f^e = \ln \lambda_f^e, \quad \varepsilon_f^v = \ln \lambda_f^v, \quad d_f^v = \dot{\lambda}_f^v / \lambda_f^v \quad (13)$$

The incremental evolution of the viscous stretch is obtained using the exponential mapping in (13d) that allows us to write

$$\lambda_{f_{n+1}}^v = \exp(\Delta t d_f^v) \lambda_{f_n}^v, \quad \text{or} \quad d_f^v = \frac{1}{\Delta t} \ln \left( \frac{\lambda_{f_{n+1}}^v}{\lambda_{f_n}^v} \right) \quad (14)$$

The novelty of this work is the inclusion of two new internal variables  $\eta$  and  $\eta^e$  both related to damage, modifying the free energy accumulated by the reinforcement. The free energy of the fibers involves two terms of the form

$$W = \varphi_f^d(\lambda_f, \eta) + \varphi_f^{ed}(\lambda_f^e, \eta^e) = (1 - \eta)\varphi_f(\lambda_f) + (1 - \eta^e)\varphi_f^e(\lambda_f^e) \quad (15)$$

The first one is related to the first branch of the fibers in Figure 1 and accounts for the elastic strain accumulated because of the total stretch  $\lambda_f$ . The second one is related to the strain energy accumulated by the second branch because of the elastic stretch  $\lambda_f^e$ . Both terms are, however, weighted by the damage variables. Finally, the dissipation potential is split in three terms. The first is related to dissipation because of viscosity and dependent on the viscous stretching  $d_f^v$ , while the second and third terms are related to dissipation because of the rate of damage variables  $\dot{\eta}$  and  $\dot{\eta}^e$ .

$$\psi = \psi_f(d_f^v) + \chi_f(\dot{\eta}; \eta) + \chi_f^e(\dot{\eta}^e; \eta^e)$$

These dissipative potentials complete the model providing the necessary information for the evolution of the internal variables  $\lambda_f^v$ ,  $\eta$ , and  $\eta^e$ .

Substituting all given potentials in (5) and rearranging terms, the incremental potential  $\Psi_f$  takes the expression

$$\Psi_f = \Psi_f^D + \Psi_f^{VD} \quad (16)$$

$$\Psi_f^D(\lambda_{f_{n+1}}) = \min_{\eta_{n+1}} \underbrace{\left\{ \Delta\varphi_f^d(\lambda_{f_{n+1}}) + \Delta t \chi_f(\dot{\eta}; \eta_{n+\alpha}) \right\}}_{\tilde{\Psi}_f^D(\lambda_{f_{n+1}}, \eta_{n+1})} \quad (17)$$

$$\Psi_f^{VD}(\lambda_{f_{n+1}}) = \min_{\lambda_{f_{n+1}}^v, \eta_{n+1}^e} \underbrace{\left\{ \Delta\varphi_f^{ed}(\lambda_{f_{n+1}}^e, \eta_{n+1}^e) + \Delta t \psi_f(d_{f_{n+1}}^v) + \Delta t \chi_f^e(\dot{\eta}^e; \eta_{n+\alpha}^e) \right\}}_{\tilde{\Psi}_f^{VD}(\lambda_{f_{n+1}}, \lambda_{f_{n+1}}^v, \eta_{n+1}^e)} \quad (18)$$

$$\Delta\varphi_f^d = (1 - \eta_{n+1})\varphi_f(\lambda_{f_{n+1}}) - (1 - \eta_n)\varphi_f(\lambda_{f_n}) \quad (19)$$

$$\Delta\varphi_f^{ed} = (1 - \eta_{n+1}^e)\varphi_f^e(\lambda_{f_{n+1}}^e) - (1 - \eta_n^e)\varphi_f^e(\lambda_{f_n}^e) \quad (20)$$

$$\dot{\eta} = \frac{\Delta\eta}{\Delta t} = \frac{\eta_{n+1} - \eta_n}{\Delta t}, \quad \dot{\eta}^e = \frac{\Delta\eta^e}{\Delta t} = \frac{\eta_{n+1}^e - \eta_n^e}{\Delta t} \quad (21)$$

Decomposition (16) expresses the additive contribution of the two fiber branches displayed in Figure 1; the first one corresponds to elastic-damage coupling, while the second one is related to the visco-elastic damage coupling. As previously mentioned, fibers are assumed to contribute in strain energy only for positive stretching and consequently take the form

$$\varphi_f = \begin{cases} \bar{\varphi}_f(\lambda_f) & \text{if } \lambda_f \geq 0 \\ 0 & \text{if } \lambda_f < 0 \end{cases}, \quad \varphi_f^e = \begin{cases} \bar{\varphi}_f^e(\lambda_f^e) & \text{if } \lambda_f^e \geq 0 \\ 0 & \text{if } \lambda_f^e < 0 \end{cases} \quad (22)$$

Similar behavior is set for the dissipation potential  $\psi_f$ , attributing a zero value for compressive viscous stretching:

$$\psi_f = \begin{cases} \bar{\psi}_f(d_f^v) & \text{if } d_f^v \geq 0 \\ 0 & \text{if } d_f^v < 0 \end{cases} \quad (23)$$

The dissipation potentials  $\chi_f$  and  $\chi_f^e$  are proposed to be homogeneous functions of degree one of  $\dot{\eta}$  and  $\dot{\eta}^e$ , respectively. This characteristic turns the response of the model (stress) independent of damage rates. Rate dependence on this variable may however be included later without any theoretical difficulty, if needed. Finally, an exact penalization for negative damage rates (increments) is included as follows:

$$\chi_f(\dot{\eta}; \eta) = \begin{cases} Y(\eta)\dot{\eta} & \text{if } \dot{\eta} \geq 0 \\ +\infty & \text{if } \dot{\eta} < 0 \end{cases}, \quad \chi_f^e(\dot{\eta}^e; \eta^e) = \begin{cases} Y^e(\eta^e)\dot{\eta}^e & \text{if } \dot{\eta}^e \geq 0 \\ +\infty & \text{if } \dot{\eta}^e < 0 \end{cases} \quad (24)$$

To end the present formalism, it is important to note that functions (24) and corresponding derivatives are evaluated in (17) and (18) at the intermediate time  $n + \alpha$ ,  $\alpha \in [0, 1]$  between  $n$  and  $n + 1$ . To this aim, we use the following approximation:

$$Y(\eta_{n+\alpha}) \simeq Y_\alpha(\eta_{n+1}) = (1 - \alpha)Y(\eta_n) + \alpha Y(\eta_{n+1}) \quad (25)$$

$$Y^e(\eta_{n+\alpha}) \simeq Y_\alpha^e(\eta_{n+1}^e) = (1 - \alpha^e)Y^e(\eta_n^e) + \alpha^e Y^e(\eta_{n+1}^e) \quad (26)$$

Parameter  $\alpha$  drives the integration algorithm from full explicit ( $\alpha = 0$ ) to full implicit ( $\alpha = 1$ ). Following the same principles discussed in [36], convenient values for  $\alpha, \alpha^e$  that minimize the time integration error can be obtained from the satisfaction of the following conditions:

$$Y(\eta_{n+1}) = Y_\alpha(\eta_{n+1}) + \alpha \frac{\partial Y(\eta_{n+1})}{\partial \eta_{n+1}} \Delta \eta, \quad Y^e(\eta_{n+1}^e) = Y_\alpha^e(\eta_{n+1}^e) + \alpha^e \frac{\partial Y^e(\eta_{n+1}^e)}{\partial \eta_{n+1}^e} \Delta \eta^e \quad (27)$$

from which the values of  $\alpha$  and  $\alpha^e$  can be explicitly expressed as

$$\alpha = \frac{Y(\eta_{n+1}) - Y(\eta_n)}{Y(\eta_{n+1}) - Y(\eta_n) + \frac{\partial Y(\eta_{n+1})}{\partial \eta_{n+1}} \Delta \eta}, \quad \alpha^e = \frac{Y^e(\eta_{n+1}^e) - Y^e(\eta_n^e)}{Y^e(\eta_{n+1}^e) - Y^e(\eta_n^e) + \frac{\partial Y^e(\eta_{n+1}^e)}{\partial \eta_{n+1}^e} \Delta \eta^e} \quad (28)$$

The influence of the parameter  $\alpha$  into the time integration error is discussed in Section 4.1.

### 3.3. Minimization operations

The isotropic minimization problem (9) was presented and studied extensively in [27]. Then, we focus here on the minimization of the fiber incremental potentials (17) and (18) coupling damage and viscosity. Both problems are constrained by the inequalities  $\Delta \eta \geq 0$  and  $\Delta \eta_e \geq 0$  coming from the exact penalization for negative increments introduced in (24).

The constrained scalar minimization problem (17) is efficiently solved by a (two step) complementarity problem. Firstly, it is calculated the slope of  $\tilde{\Psi}_f^D$  at the origin  $\eta_{n+1} = \eta_n$  (i.e.,  $\Delta \eta = 0$ ). If the derivative is strictly negative, then there exists  $\Delta \eta > 0$  that solves the minimization problem. Conversely, the minimizer is  $\Delta \eta = 0$ , i.e., no damage increment exists within the load step. This procedure is then similar to a damage yield function evaluation:

$$s = \left. \frac{\partial \tilde{\Psi}_f^D}{\partial \eta_{n+1}} \right|_{\eta_{n+1}=\eta_n} = -\varphi_f(\lambda_{f_{n+1}}) + Y(\eta_n) \tag{29}$$

if  $s < 0$  then,  $\Delta\eta > 0$ ; else,  $\Delta\eta = 0$

In case that  $\Delta\eta > 0$ , the optimality condition provides the nonlinear equation in  $\eta_{n+1}$  to be solved:

$$\begin{aligned} r(\eta_{n+1}) &= \frac{\partial \tilde{\Psi}_f^D}{\partial \eta_{n+1}} = -\varphi_f(\lambda_{f_{n+1}}) + \Delta t \frac{\partial \chi_f(\eta_{n+1})}{\partial \eta_{n+1}} \\ &= -\varphi_f(\lambda_{f_{n+1}}) + Y_\alpha + \frac{\partial Y_\alpha}{\partial \eta_{n+1}} \Delta\eta = 0 \end{aligned} \tag{30}$$

Using Newton method to find the root  $x = \eta_{n+1}$  we have the recursive formula

$$x^{k+1} = x^k + \Delta x, \quad K^k \Delta x = -r^k \tag{31}$$

$$K(\eta_{n+1}) = \frac{\partial r}{\partial \eta_{n+1}} = 2 \frac{\partial Y_\alpha}{\partial \eta_{n+1}} + \Delta\eta \frac{\partial^2 Y_\alpha}{\partial \eta_{n+1}^2} \tag{32}$$

The expressions for  $r(\eta_{n+1})$  and  $K(\eta_{n+1})$  can be further simplified if  $Y_\alpha$  is substituted by (25) and  $\alpha$  is chosen to take the value given by (28a). In this case, both quantities become conveniently independent of the parameter  $\alpha$ :

$$r(\eta_{n+1}) = -\varphi_f(\lambda_{f_{n+1}}) + Y(\eta_{n+1}) = 0 \tag{33}$$

$$K(\eta_{n+1}) = \frac{\partial Y(\eta_{n+1})}{\partial \eta_{n+1}} \tag{34}$$

which means that an expression for the residual that is independent of the integration parameter.

The minimization problem (18) associated with the branch VED in Figure 1 involves two simultaneous internal variables: viscous stretch  $\lambda_{f_{n+1}}^v = \lambda_{f_n}^v + \Delta\lambda^v$  and damage  $\eta_{n+1}^e = \eta_n^e + \Delta\eta^e$ , with  $\Delta\eta^e \geq 0$ . Assuming that problem (18) is a convex function of its arguments, the minimization procedure is conveniently set up as follows: Firstly, Equation (18) is minimized with respect to the viscous stretch  $\lambda_{f_{n+1}}^v$  assuming no damage increment, i.e., fixed value  $\eta_{n+1}^e = \eta_n^e$  and  $\Delta\eta^e = 0$ . The minimizer is then given by

$$\bar{\lambda}_{f_{n+1}}^v = \arg \min_{\lambda_{f_{n+1}}^v} \left\{ \Delta\varphi_f^{ed}(\lambda_{f_{n+1}}^e, \eta_n^e) + \Delta t \psi_f(d_{f_{n+1}}^v) \right\} \tag{35}$$

Operational details of this minimization due to the definition of potentials  $\varphi_f^{ed}$  and  $\psi_f$  are discussed in [29]. Once the minimizing argument  $\bar{\lambda}_{f_{n+1}}^v$  was achieved, the derivative of  $\tilde{\Psi}_f^{VD}$  with respect to  $\eta_{n+1}^e$  is evaluated, providing a damage yield evaluation analogous to (29):

$$s = \left. \frac{\partial \tilde{\Psi}_f^{VD}}{\partial \eta_{n+1}^e} \right|_{\eta_{n+1}^e=\eta_n^e} = -\varphi_f^e(\bar{\lambda}_{f_{n+1}}^v) + Y^e(\eta_n^e) \tag{36}$$

if  $s < 0$  then,  $\Delta\eta^e > 0$ ; else,  $\Delta\eta^e = 0$

In other words, if the slope  $s$  is nonnegative, a local (global) minimum has been reached at  $\Delta\eta^e = 0$  and no damage increment occurs in this branch. In this case, the internal variables update as follows:  $\lambda_{f_{n+1}}^v = \bar{\lambda}_{f_{n+1}}^v$  and  $\eta_{n+1}^e = \eta_n^e$ . Conversely, if  $s$  is strictly negative, then there exists  $\Delta\eta^e > 0$  that satisfies the solution of (18), and the corresponding optimality conditions are given by

$$\begin{aligned}
 r_1 &= \frac{\partial \tilde{\Psi}_f^{VD}}{\partial \lambda_{f_{n+1}}^v} = (1 - \eta_{n+1}^e) \frac{\partial \varphi_f^e(\lambda_{f_{n+1}}^e)}{\partial \lambda_{f_{n+1}}^v} + \Delta t \frac{\psi_f(d_{f_{n+1}}^v)}{\partial \lambda_{f_{n+1}}^v} \\
 &= (1 - \eta_{n+1}^e) \frac{\partial \varphi_f^e}{\partial \lambda_{f_{n+1}}^e} \left( -\frac{\lambda_{f_{n+1}}}{\lambda_{f_{n+1}}^v} \right) + \frac{\psi_f}{\partial d_{f_{n+1}}^v} \frac{1}{\lambda_{f_{n+1}}^v} = 0
 \end{aligned}
 \tag{37}$$

$$r_2 = \frac{\partial \tilde{\Psi}_f^{VD}}{\partial \eta_{n+1}^e} = -\varphi_f^e(\lambda_{f_{n+1}}^e) + Y_\alpha^e + \alpha^e \frac{\partial Y^e(\eta_{n+1}^e)}{\partial \eta_{n+1}^e} \Delta \eta^e = 0
 \tag{38}$$

Calling  $\mathbf{r} = \{r_1, r_2\}$  and using Newton method to find the roots  $\mathbf{x} = \{\lambda_{f_{n+1}}^v, \eta_{n+1}^e\}$ , we have the recursive formula

$$\mathbf{x}^{k+1} = \mathbf{x}^k + \Delta \mathbf{x}, \quad \mathbf{K}^k \Delta \mathbf{x} = -\mathbf{r}^k, \quad \mathbf{K} = \begin{bmatrix} K_{11} & H \\ H & K_{22} \end{bmatrix}
 \tag{39}$$

$$K_{11} = \frac{\partial r_1}{\partial \lambda_{f_{n+1}}^v} = (1 - \eta_{n+1}^e) \left[ \frac{\partial^2 \varphi_f^e}{\partial \lambda_{f_{n+1}}^e} \frac{\lambda_{f_{n+1}}^2}{\lambda_{f_{n+1}}^v} + \frac{\partial \varphi_f^e}{\partial \lambda_{f_{n+1}}^e} \frac{\lambda_{f_{n+1}}}{\lambda_{f_{n+1}}^v} \right] + \frac{\partial^2 \psi_f}{\partial d_{f_{n+1}}^v} \frac{1}{\Delta t} \frac{1}{\lambda_{f_{n+1}}^v}
 \tag{40}$$

$$K_{22} = \frac{\partial r_2}{\partial \eta_{n+1}^e} = 2\alpha^e \frac{\partial Y^e(\eta_{n+1}^e)}{\partial \eta_{n+1}^e} + \alpha^e \frac{\partial^2 Y^e(\eta_{n+1}^e)}{\partial \eta_{n+1}^e} \Delta \eta^e
 \tag{41}$$

$$H = \frac{\partial r_1}{\partial \eta_{n+1}^e} = \frac{\partial r_2}{\partial \lambda_{f_{n+1}}^v} = -\frac{\partial \varphi_f^e}{\partial \lambda_{f_{n+1}}^e} \frac{\lambda_{f_{n+1}}}{\lambda_{f_{n+1}}^v}
 \tag{42}$$

Once again, the expressions for  $\mathbf{r}(\eta_{n+1})$  and  $\mathbf{K}(\eta_{n+1})$  can be further simplified if  $Y_\alpha^e$  is substituted by (26) and  $\alpha^e$  is chosen to take the value given by (28b) rendering both quantities independent of  $\alpha^e$ :

$$r_1 = (1 - \eta_{n+1}^e) \frac{\partial \varphi_f^e}{\partial \lambda_{f_{n+1}}^e} \left( -\frac{\lambda_{f_{n+1}}}{\lambda_{f_{n+1}}^v} \right) + \frac{\psi_f}{\partial d_{f_{n+1}}^v} \frac{1}{\lambda_{f_{n+1}}^v} = 0
 \tag{43}$$

$$r_2 = -\varphi_f^e(\lambda_{f_{n+1}}^e) + Y^e(\eta_{n+1}^e) = 0
 \tag{44}$$

$$K_{11} = (1 - \eta_{n+1}^e) \left[ \frac{\partial^2 \varphi_f^e}{\partial \lambda_{f_{n+1}}^e} \frac{\lambda_{f_{n+1}}^2}{\lambda_{f_{n+1}}^v} + \frac{\partial \varphi_f^e}{\partial \lambda_{f_{n+1}}^e} \frac{\lambda_{f_{n+1}}}{\lambda_{f_{n+1}}^v} \right] + \frac{\partial^2 \psi_f}{\partial d_{f_{n+1}}^v} \frac{1}{\Delta t} \frac{1}{\lambda_{f_{n+1}}^v}
 \tag{45}$$

$$K_{22} = \frac{\partial Y^e(\eta_{n+1}^e)}{\partial \eta_{n+1}^e} \quad H = -\frac{\partial \varphi_f^e}{\partial \lambda_{f_{n+1}}^e} \frac{\lambda_{f_{n+1}}}{\lambda_{f_{n+1}}^v}
 \tag{46}$$

Once all minimizers are found, the first Piola–Kirchhoff stress tensor is calculated by the hyperelastic-like expression (4). After substitution of potentials, it is conveniently rewritten as

$$\begin{aligned} \mathbf{P}_{n+1} &= \mathbf{F}_{n+1} \mathbf{S}_{n+1} = 2\mathbf{F}_{n+1} \frac{\partial \Psi(\mathbf{C}_{n+1}; \xi_n)}{\partial \mathbf{C}_{n+1}} \\ &= \mathbf{F}_{n+1} \left[ 2J_{n+1}^{-2/3} \text{DEV} \left( \frac{\partial}{\partial \hat{\mathbf{C}}_{n+1}} \left( \varphi + \varphi^e + \varphi_f^d + \varphi_f^{ed} \right) \right) + \frac{\partial U}{\partial J_{n+1}} J_{n+1} \mathbf{C}_{n+1}^{-1} \right] \end{aligned} \tag{47}$$

where  $\text{DEV}(\cdot) = (\cdot) - 1/3[(\cdot) : \mathbf{C}]\mathbf{C}^{-1}$  and  $\mathbf{S}$  is the second Piola–Kirchhoff stress tensor, which may be decomposed into a volumetric and an isochoric part by

$$\mathbf{S} = \mathbf{S}_{vol} + \bar{\mathbf{S}} \tag{48}$$

such as

$$\mathbf{S}_{vol} = \frac{\partial U}{\partial J} J \mathbf{C}^{-1} \tag{49}$$

$$\bar{\mathbf{S}} = J^{-2/3} \text{DEV} \left( 2 \frac{\partial}{\partial \hat{\mathbf{C}}} \left( \varphi + \varphi^e + \varphi_f^d + \varphi_f^{ed} \right) \right) = J^{-2/3} \text{DEV}(\hat{\mathbf{S}}) \tag{50}$$

where

$$\hat{\mathbf{S}} = 2 \frac{\partial \left( \varphi + \varphi^e + \varphi_f^d + \varphi_f^{ed} \right)}{\partial \hat{\mathbf{C}}} \tag{51}$$

### 3.4. Specific material models

Provided that the general constitutive framework set up by Equations (9), (17), and (18), different mechanical behaviors can be obtained depending on the specific expressions for the potentials. For the isotropic contribution (9), any convenient hyperelastic law like Neo–Hookean, Mooney–Rivlin, Ogden, and Hencky models can be used. Hencky expressions are of the type

$$\varphi = \mu \sum_{j=1}^3 (\varepsilon_j)^2, \quad \varphi^e = \mu^e \sum_{j=1}^3 (\varepsilon_j^e)^2, \quad \psi = \eta^v \sum_{j=1}^3 (d_j^v)^2 \tag{52}$$

while the Ogden expressions are written as

$$\varphi = \sum_{j=1}^3 \sum_{p=1}^N \frac{\mu_p}{\alpha_p} \left( [\exp(\varepsilon_j)]^{\alpha_p} - 1 \right) \tag{53}$$

$$\varphi^e = \sum_{j=1}^3 \sum_{p=1}^N \frac{\mu_p^e}{\alpha_p} \left( [\exp(\varepsilon_j^e)]^{\alpha_p} - 1 \right) \tag{54}$$

$$\psi = \sum_{j=1}^3 \sum_{p=1}^N \frac{\eta_p^v}{\alpha_p} \left( [\exp(d_j^v)]^{\alpha_p} - 1 \right) \tag{55}$$

Symbols  $\mu, \mu^e, \eta^v, \mu_p, \mu_p^e, \mu_p^v,$  and  $\alpha_p$  are material parameters to be identified. More details on this issue are found in [27].

For the reinforcement hyperelastic potentials  $\bar{\varphi}_f$  and  $\bar{\varphi}_f^e$ , we chose here the classical exponential function proposed in [11]:

$$\bar{\varphi}_f = \frac{k_1}{2k_2} \left\{ \exp \left[ k_2 (I_f - 1)^2 \right] - 1 \right\}, \quad \bar{\varphi}_f^e = \frac{k_1^e}{2k_2^e} \left\{ \exp \left[ k_2^e (I_f^e - 1)^2 \right] - 1 \right\} \tag{56}$$

where  $I_f = \lambda_f^2, \quad I_f^e = (\lambda_f^e)^2$ . For the dissipative potential  $\bar{\psi}_f$ , the quadratic Hencky-type law (52) showed to be adequate.

A key issue in the present context is the evolution of the damage internal variables  $\eta$  and  $\eta^e$ . In the pioneer study of [8], a damage yield surface is completely determined by the maximum attained strain level and uses the square root of the undamaged strain energy (equivalent strain) as an intermediate variable (approach that was followed by a wide set of works [16–18]). In the present variational setting, the damage evolution arises as a direct consequence of the internal variables minimization. This operation controls the two common questions involved: whether or not a damage increment occurs (related to a damage yield surface) and its amplitude in case of existence. The minimizing values, indeed, are strongly dependent on the energy-like functions  $Y(\eta)$ ,  $Y^e(\eta^e)$  whose choice is based on their capacity of reproducing experimental data. Two expressions are proposed here. The first is a simple potential function, while the second provides a penalization for damage accumulation (i.e., when  $\eta \rightarrow 1$ ):

$$Y(\eta) = \zeta_0 + \zeta \eta^p \tag{57}$$

$$Y(\eta) = \zeta_0 + \beta [-\ln(1 - \eta)]^\gamma \tag{58}$$

Constants  $\zeta_0$ ,  $\zeta$ ,  $p$ ,  $\beta$ , and  $\gamma$  are material parameters.

For these potentials, the derivatives of (47) and (50) take the particular expressions (Appendix)

$$\frac{\partial \varphi}{\partial \hat{\mathbf{C}}_{n+1}} = \sum_{j=1}^3 \frac{\partial \varphi}{\partial c_j} \mathbf{E}_j = \sum_{j=1}^3 \frac{\partial \varphi}{\partial \varepsilon_j^e} \frac{1}{2c_j} \mathbf{E}_j \tag{59}$$

$$\frac{\partial \varphi^e}{\partial \hat{\mathbf{C}}_{n+1}} = \hat{\mathbf{F}}_n^{v-1} \left( \sum_{j=1}^3 \frac{\partial \varphi^e}{\partial \varepsilon_j^e} \frac{1}{2c_j^{pr}} \mathbf{E}_j^{pr} \right) \hat{\mathbf{F}}_n^{v-T} \tag{60}$$

$$\frac{\partial \varphi_f^d}{\partial \hat{\mathbf{C}}_{n+1}} = (1 - \eta_{n+1}) \frac{1}{2\lambda_{f_{n+1}}} \frac{\partial \varphi_f}{\partial \lambda_{f_{n+1}}} \mathbf{A}_f \tag{61}$$

$$\frac{\partial \varphi_f^{ed}}{\partial \hat{\mathbf{C}}_{n+1}} = (1 - \eta_{n+1}^e) \frac{1}{2(\lambda_{f_{n+1}} \lambda_{f_{n+1}}^v)} \frac{\partial \varphi_f^e}{\partial \lambda_{f_{n+1}}^e} \mathbf{A}_f \tag{62}$$

### 3.5. Elasticity tensor

The analytic expression for the elasticity tensor (tangent modulus) is important to solve a linearized nonlinear finite element problem. Because the present model is based on an additive decomposition of the energy, the elasticity tensor may be written in a decoupled form:

$$\mathbb{C} = \mathbb{C}_{vol} + \bar{\mathbb{C}} \tag{63}$$

such as

$$\mathbb{C}_{vol} = 2 \frac{\partial \mathbb{S}_{vol}}{\partial \mathbb{C}} \tag{64}$$

$$\bar{\mathbb{C}} = 2 \frac{\partial \bar{\mathbb{S}}}{\partial \mathbb{C}} \tag{65}$$

where the operations to obtain the geometric terms are common to any hyperelastic model. Thus, the focus here is on the expression of the incremental material tensor:

$$\hat{\mathbb{C}} = \frac{\partial \hat{\mathbb{S}}_{n+1}}{\partial \hat{\mathbb{C}}_{n+1}} = \frac{d}{d \hat{\mathbb{C}}_{n+1}} \left( \frac{\partial \Psi}{\partial \hat{\mathbb{C}}_{n+1}} \right) \tag{66}$$

$$= \frac{d}{d\hat{\mathbf{C}}_{n+1}} \left( \frac{\partial \Psi_{iso}}{\partial \hat{\mathbf{C}}_{n+1}} + \frac{\partial \Psi_f}{\partial \hat{\mathbf{C}}_{n+1}} \right) \tag{67}$$

where the first term, related to the isotropic part, is presented in detail in [27]. The second term is obtained by

$$\hat{\mathbf{C}}_f = \frac{d}{d\hat{\mathbf{C}}_{n+1}} \left( \frac{\partial \Psi_f}{\partial \hat{\mathbf{C}}_{n+1}} \right) = \frac{d}{d\hat{\mathbf{C}}_{n+1}} \left( \frac{\partial \Psi_f^D}{\partial \hat{\mathbf{C}}_{n+1}} + \frac{\partial \Psi_f^{VD}}{\partial \hat{\mathbf{C}}_{n+1}} \right) \tag{68}$$

$$= \frac{d}{d\hat{\mathbf{C}}_{n+1}} \left( \frac{\partial \varphi_f^d}{\partial \hat{\mathbf{C}}_{n+1}} \right) + \frac{d}{d\hat{\mathbf{C}}_{n+1}} \left( \frac{\partial \varphi_f^{ed}}{\partial \hat{\mathbf{C}}_{n+1}} \right) \tag{69}$$

such that

$$\frac{d}{d\hat{\mathbf{C}}_{n+1}} \left( \frac{\partial \varphi_f^d}{\partial \hat{\mathbf{C}}_{n+1}} \right) = (1 - \eta_{n+1}) \left( \frac{\partial^2 \varphi_f}{\partial \lambda_{f_{n+1}}^2} \frac{1}{4\lambda_{f_{n+1}}^2} - \frac{\partial \varphi_f}{\partial \lambda_{f_{n+1}}} \frac{1}{4\lambda_{f_{n+1}}^3} \right) \mathbb{A} \tag{70}$$

$$\begin{aligned} \frac{d}{d\hat{\mathbf{C}}_{n+1}} \left( \frac{\partial \varphi_f^{ed}}{\partial \hat{\mathbf{C}}_{n+1}} \right) &= (1 - \eta_{n+1}^e) \frac{1}{2\lambda_{f_{n+1}}} \left( \frac{\partial^2 \varphi_f^e}{\partial \lambda_{f_{n+1}}^2} \frac{d\lambda_{f_{n+1}}^e}{d\lambda_{f_{n+1}}} \frac{\lambda_{f_{n+1}}^e}{2\lambda_{f_{n+1}}^2} + \right. \\ &\left. + \frac{\partial \varphi_f^e}{\partial \lambda_{f_{n+1}}} \frac{d\lambda_{f_{n+1}}^e}{d\lambda_{f_{n+1}}} \frac{1}{2\lambda_{f_{n+1}}^2} - \frac{\partial \varphi_f^e}{\partial \lambda_{f_{n+1}}} \frac{\lambda_{f_{n+1}}^e}{2\lambda_{f_{n+1}}^3} \right) \mathbb{A} \end{aligned} \tag{71}$$

where  $\mathbb{A}_{ijkl} = \mathbf{a}_{f_i} \mathbf{a}_{f_j} \mathbf{a}_{f_k} \mathbf{a}_{f_l}$  and  $\frac{d\lambda_{f_{n+1}}^e}{d\lambda_{f_{n+1}}}$  is obtained with the same procedure proposed in [34]:

$$\frac{d\lambda_{f_{n+1}}^e}{d\lambda_{f_{n+1}}} = \frac{\partial^2 \psi_f}{\partial d_{f_{n+1}}^v} \frac{1}{\Delta t \lambda_{f_{n+1}}} \left( \frac{\partial^2 \psi_f}{\partial d_{f_{n+1}}^v} \frac{1}{\Delta t \lambda_{f_{n+1}}^e} + \frac{\partial^2 \varphi_f^e}{\partial \lambda_{f_{n+1}}^e} \lambda_{f_{n+1}}^e + \frac{\partial \varphi_f^e}{\partial \lambda_{f_{n+1}}^e} \right)^{-1} \tag{72}$$

#### 4. NUMERICAL EXAMPLES

The objective of this section is to show a set of examples illustrating the main features of the proposed model. In Section 4.1, the efficacy of the proposed time integration scheme for parameter  $\alpha$  is studied. In Section 4.2, examples focusing the constitutive model and exploring its main features due to different loading histories are shown. The last example shows its implementation in the academic finite element code METAFOR [37] – developed by LTAS, ULg, Belgium.

##### 4.1. Tests on the time integration procedure

The time integration scheme (27) depends on the parameter  $\alpha$  leading to different errors when the time increment is not small enough. However, convenient automatic values can be computed by the proposed expression (28). Figure 2 shows the stress–strain curves for a loading–unloading cycle using  $\alpha = 0.25$ ,  $\alpha = 0.60$ ,  $\alpha = 1.00$ , and the automatic calculated value (Equation (28)). All cases converge to the same curve when the  $\Delta t$  goes to 0, i.e., small strain increments. Figure 3 shows the convergence of the accumulated damage for different values of  $\alpha$  as the time increment decreases. It is possible to see that the automatic procedure is able to accurately represent damage evolution and the accumulated damage value even for large time increments.

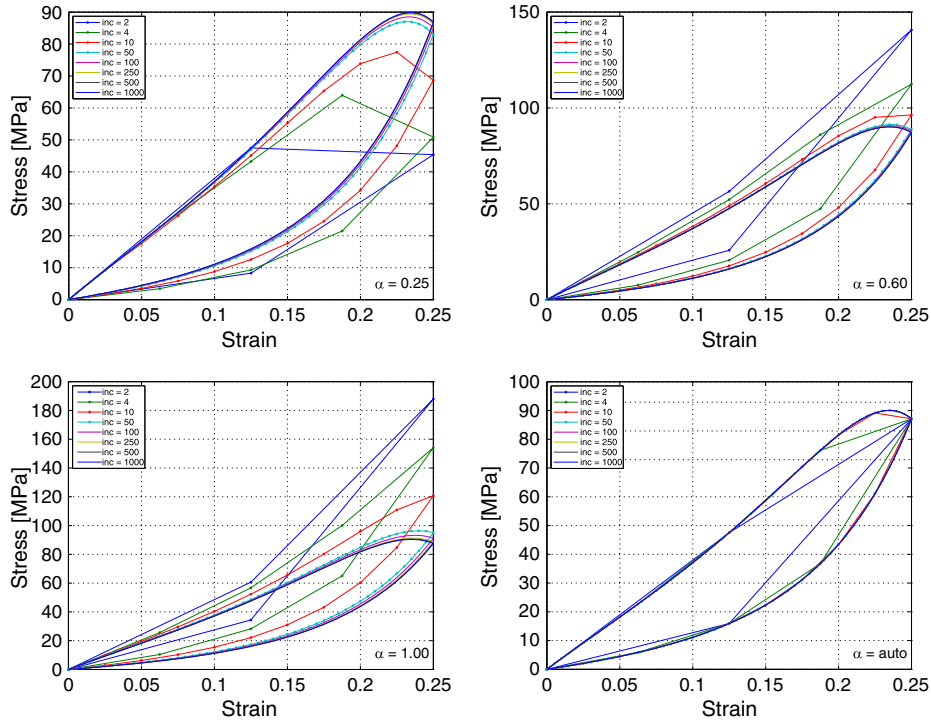


Figure 2. Stress–strain curve for a loading–unloading cycle using different values for  $\alpha$ .

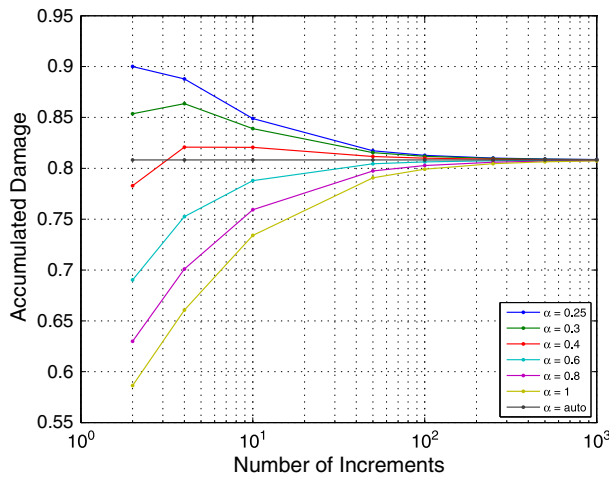


Figure 3. Convergence of the accumulated damage for different values of  $\alpha$ .

4.2. Uniaxial cases

Aiming to test the damage capabilities of the proposed model, a set of uniaxial tests were performed considering exclusively the branches associated with the fiber contribution (Figure 1). Two uniaxial stretching tests at controlled strain rate were performed on the fiber direction. The first one is performed using the elastic-damage branch of the model only, related to Equation (17), while the second is performed with the viscous elastic-damage branch only, related to Equation (18). The potentials used and corresponding parameters are shown in Table I. The applied strain and the resulting stress–strain curve for each case are displayed in Figure 4. Figure 4(a) shows the elastic-damage case within a cyclic test with bounded maximum strain providing an unloading curve always followed by the subsequent loadings. Figure 4(b) shows the elastic-damage case within a

Table I. Material parameters of the uniaxial cases for the fiber contribution.

Potential	Fiber	
	Model	Parameters
$\varphi_f$	Holzappel	$k_1 = 100 \text{ MPa}$ e $k_2 = 3$
$Y$	Equation (57)	$\zeta = 50 \text{ MPa}$ e $p = 3$
$\varphi_f^e$	Holzappel	$k_1 = 100 \text{ MPa}$ e $k_2 = 3$
$\psi_f$	Hencky	$\eta^v = 5000 \text{ MPa} \cdot \text{s}^{-1}$
$Y^e$	Equation (57)	$\zeta = 50 \text{ MPa}$ e $p = 3$

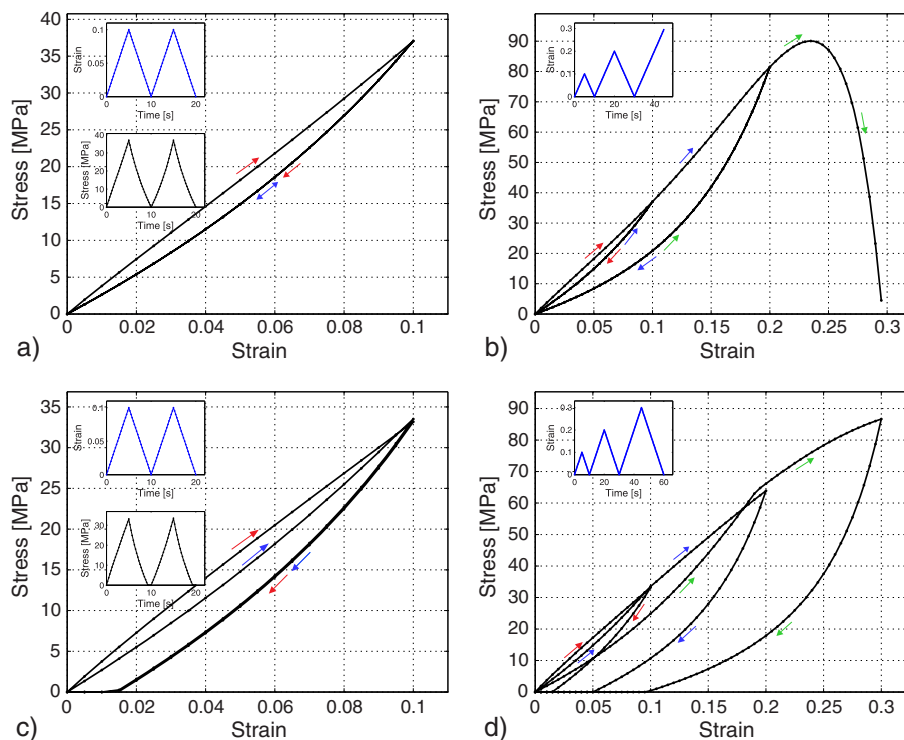


Figure 4. Stress–strain curves for a loading–unloading cycles for different strain histories. First loading/unloading cycle (red). Second loading/unloading cycle (blue). Third loading/unloading cycle (green).

cyclic test with growing maximum strain. It is possible to see that the reloading curves are always twofold. A first purely elastic up to the maximum previously attained strain and a second one with increasing damage.

Figure 4(c) and (d), on the other hand, shows the same mechanical tests performed before with the inclusion of viscous effects. In these cases, the unloading and loading cases, even without growing damage do not follow exactly the same curve. These two contributions are combined in order to represent more complex mechanical behaviors.

#### 4.3. Three-dimensional case

This example represents a cylindrical tube composed of a viscoelastic isotropic matrix and helical viscoelastic fibers allowing damage [11]. The fiber contribution uses same potentials and parameters of Table I, while the isotropic contribution uses Hencky model with a constant value of  $\mu = 50 \text{ MPa}$ . Note that the choice of Hencky expression in this example (quadratic form of its arguments) was due to simplicity reasons, because it requires a single parameter only. However, any arbitrary hyperelastic form could be used instead, depending on the needs required by experimental

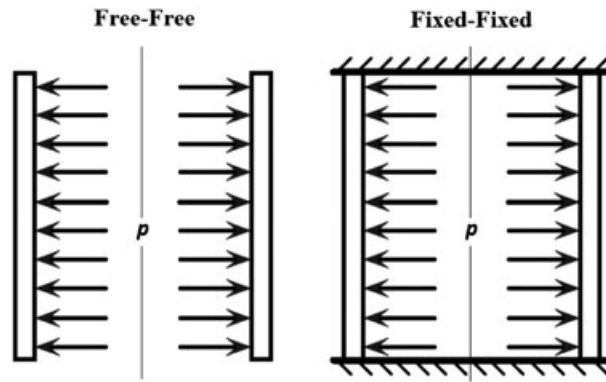


Figure 5. Boundary conditions of the cylindrical tube.

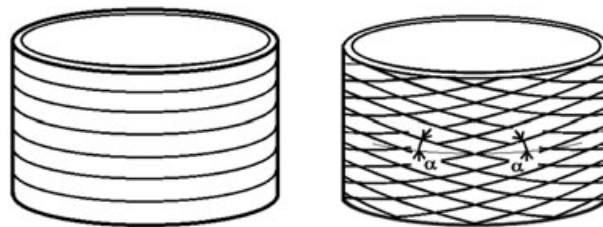


Figure 6. Tubes with a single layer with one fiber family aligned to the circumferential direction (left); single orthotropic layer with two helically arranged fiber families with a angle  $\alpha$  in respect to the circumferential direction.

observations. The wall thickness is 1 mm; the outside radius is 100 mm. Four cases are tested simulating an increasing internal pressure. Two cases are subject fixed axial displacement at the tube ends, while the other two cases are unrestricted, as shown in Figure 5. Each boundary condition cases are evaluated using two different fiber directions: circumferential (perpendicular to the axis) and orthotropic (balanced angle ply) with two continuous family of fibers helically arranged at an angle of  $\alpha = 30^\circ$  of the circumferential direction, as shown in Figure 6.

Undeformed and deformed configurations for fixed and free axial displacement with helical fibers are shown in Figure 7 (the corresponding configurations for circumferential fibers are similar).

The stress–strain curves for each case that are presented in Figures 8 and 9 show agreement with the kinematic restrictions. The cases allowing axial displacement (Figure 8) present circumferential stresses only. Mechanical damage appears clearly on the loading–unloading curves. On other hand, the cases with constrained axial displacements show both circumferential and axial stresses (Figure 8). As expected, only the helical case shows damage in the axial direction.

#### 4.4. Parameter identification

In [38], the experimental stress–strain curves of a mouse skin submitted to monotonic and cyclic uniaxial loadings at a strain rate of  $0.01 \text{ s}^{-1}$  are presented. These curves suggest that both viscous behavior and elastic softening are simultaneously present. A parameter identification was then performed in order to evaluate the capability of the present model to account for both phenomena and reproduce the experimental data.

The simulations were carried out considering that the experimental curves were obtained with fibers aligned in the loading direction. A merit function based on the square difference between the experimental and numerical data was minimized. Both monotonic and cyclic curves were simultaneously considered in the merit function, a fact that significantly increases the difficulties associated with a good model representation of the experimental data.

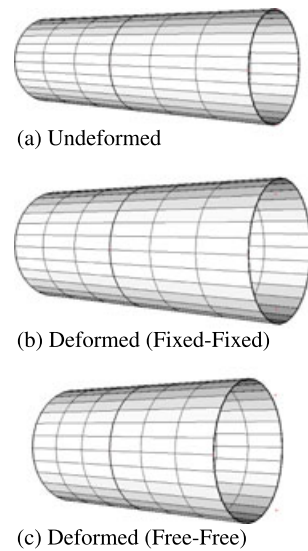


Figure 7. Configurations of the numerical simulations of a cyclic inflation of a thin-walled tube.

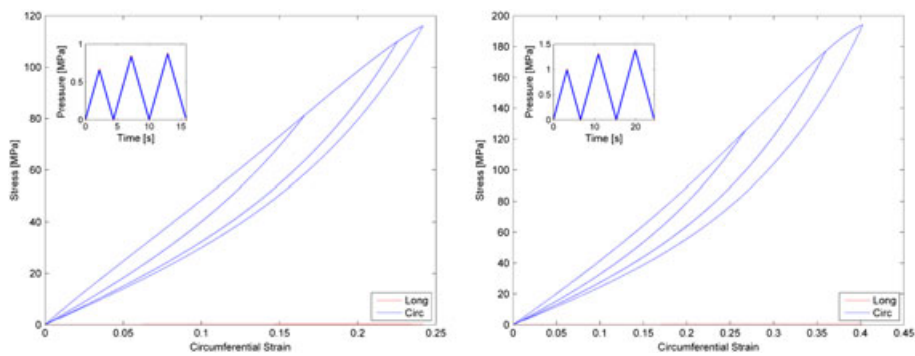


Figure 8. Tube with free axial displacements. Axial and circumferential stresses for tube with circumferential fibers (left) and helical fibers (right).

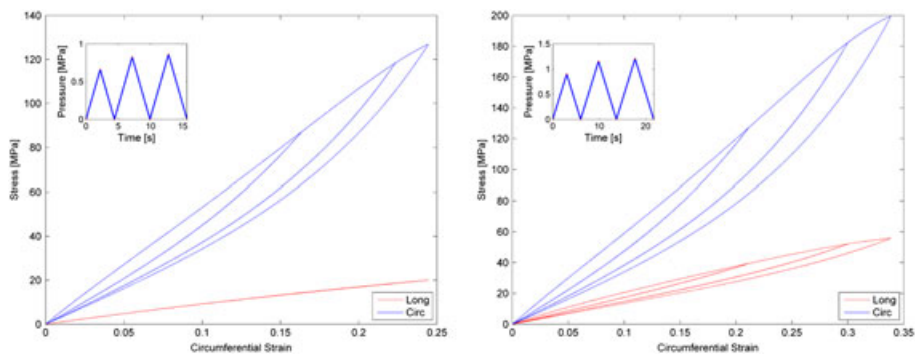


Figure 9. Tube with fixed axial displacements. Axial and circumferential stresses for tube with circumferential fibers (left) and helical fibers (right).

Table II shows the values obtained by the identification procedure. Figure 10 displays the experimental and simulated curves showing quite satisfactory results, considering the complexity of the behavior.

Table II. Material parameters of the experimental data fitting.

Potential	Model	Parameters	
$\Psi_{iso}$	$\varphi^e$ Hencky	$\mu^e = 3.57E-01$ MPa	
	$\psi$ Hencky	$\eta^v = 2.76E+00$ MPa · s <sup>-1</sup>	
$\Psi_f$	$\varphi_f$ Holzapfel	$k_1 = 5.72E-01$ MPa;	$k_2 = 1.00E+01$
	$\dot{Y}$ Equation (58)	$\beta = 2.68E-02$	$\gamma = 3.15 E+00$
	$\varphi_f^e$ Holzapfel	$k_1 = 6.15E-03$ MPa;	$k_2 = 2.27E+02$
	$\psi_f$ Equation (57)	$\zeta = 6.84E+02$ MPa · s <sup>-1</sup> ;	$p = 3.20E+00$

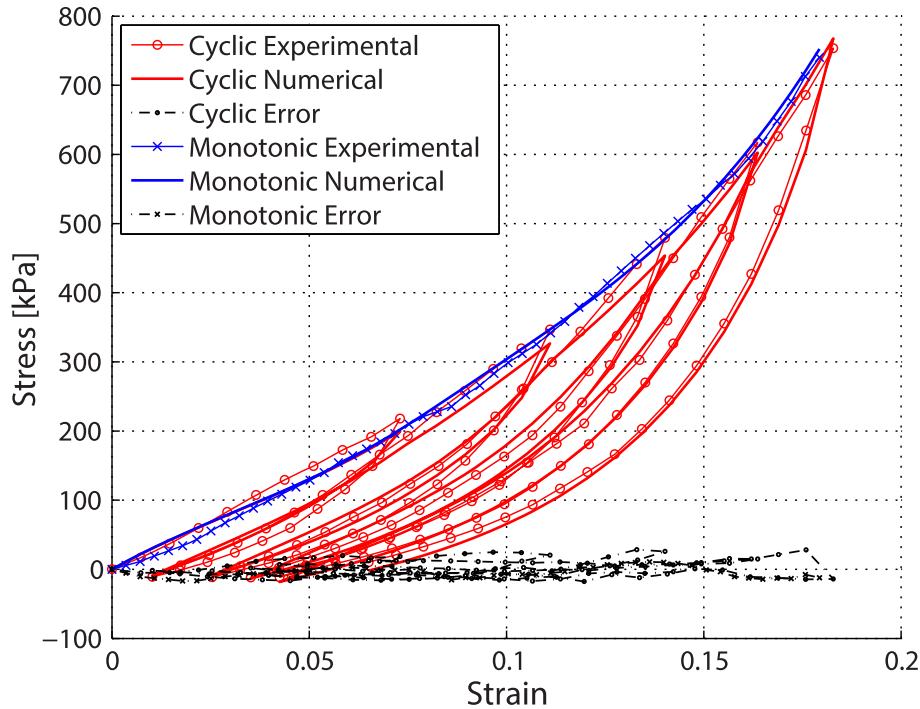


Figure 10. Experimental data fitting for mouse skin.

### 5. CONCLUSIONS

A variational constitutive model for fibrous soft materials that simultaneously accounts for nonlinear viscoelastic effects and mechanical damage of the fiber reinforcement was presented. This model should be considered as an updating of a previous one [29] turning it capable to represent the elastic softening frequently observed in these type of materials, in particular, soft fibrous biological tissues.

The model is classified as variational because the incremental problem is set up as the minimization of an incremental potential with respect to the dissipative internal variables: viscous deformation and damage. This mathematical framework allows for a straightforward choice of the hyperelastic and dissipative potentials that better represent the experimental data. From an operational point of view, the corresponding algorithm mimics the classical returning mapping schemes based on Newton’s method having the additional advantage of relating the residual reduction with the optimality condition of a convex minimization problem. Several numerical tests (a) assessed the capability of the proposed model to properly reproduce rate dependency as well as the Mullins’ effect, (b) verified that the proposed time-integration scheme embedded in the incremental potential definition allowed for large time increments without losing accuracy, and (c) showed that the model is flexible enough to mimic experimentally obtained stress–strain cyclic curves of soft tissues.

## APPENDIX A: MATERIAL MODELS

## A.1. Hencky model

Hencky model is commonly used to model the behavior of vulcanized rubber. The model has a strain energy identical to infinitesimal elasticity.

$$\varphi = \sum_{j=1}^3 \mu (\epsilon_j)^2 \quad \varphi^e = \sum_{j=1}^3 \mu^e (\epsilon_j^e)^2 \quad \psi = \sum_{j=1}^3 \eta^v (d_j^v)^2 \quad (\text{A.1})$$

$$\frac{\partial \varphi}{\partial \epsilon_j} = 2\mu \epsilon_j \quad \frac{\partial \varphi^e}{\partial \epsilon_j^e} = 2\mu^e \epsilon_j^e \quad \frac{\partial \psi}{\partial d_j^v} = 2\eta^v d_j^v \quad (\text{A.2})$$

## A.2. Ogden model

The Ogden model is usually chosen because of its flexibility in representing polymeric materials. For the isotropic contribution, the following expressions are used

$$\begin{aligned} \varphi &= \sum_{j=1}^3 \sum_{p=1}^N \frac{\mu_p}{\alpha_p} \left( [\exp(\epsilon_j)]^{\alpha_p} - 1 \right) & \varphi^e &= \sum_{j=1}^3 \sum_{p=1}^N \frac{\mu_p^e}{\alpha_p} \left( [\exp(\epsilon_j^e)]^{\alpha_p} - 1 \right) \\ \psi &= \sum_{j=1}^3 \sum_{p=1}^N \frac{\eta_p^v}{\alpha_p} \left( [\exp(d_j^v)]^{\alpha_p} - 1 \right) \end{aligned} \quad (\text{A.3})$$

$$\frac{\partial \varphi}{\partial \epsilon_j} = \sum_{p=1}^N \mu_p [\exp(\epsilon_j)]^{\alpha_p} \quad \frac{\partial \varphi^e}{\partial \epsilon_j^e} = \sum_{p=1}^N \mu_p^e [\exp(\epsilon_j^e)]^{\alpha_p} \quad \frac{\partial \psi}{\partial d_j^v} = \sum_{p=1}^N \eta_p^v [\exp(d_j^v)]^{\alpha_p} \quad (\text{A.4})$$

## A.3. Holzapfel model

In [11], a hyperelastic model is presented in which the fibrous medium (collagen/elastin) is governed by a potential of type

$$\varphi = \frac{k_1}{2k_2} \exp \left\{ [k_2(I_f - 1)^2] - 1 \right\} \quad \varphi^e = \frac{k_1}{2k_2} \exp \left\{ \left[ k_2 \left( I_f^e - 1 \right)^2 \right] - 1 \right\} \quad (\text{A.5})$$

where  $I_f^e = (\lambda_f^e)^2$ . Note again that these expressions are null, respectively, for  $\lambda_f \leq 1$  and  $\lambda_f^e \leq 1$ .

$$\begin{aligned} \frac{\partial \varphi}{\partial \lambda_f} &= k_1 \left( \exp \left( k_2 (\lambda_f^2 - 1)^2 \right) (\lambda_f^2 - 1) 2\lambda_f \right) \\ \frac{\partial \varphi^e}{\partial \lambda_f^e} &= k_1 \left( \exp \left( k_2 \left( (\lambda_f^e)^2 - 1 \right)^2 \right) \left( (\lambda_f^e)^2 - 1 \right) 2\lambda_f^e \right) \end{aligned} \quad (\text{A.6})$$

## APPENDIX B

$$Y(\eta_{n+\alpha}) \simeq Y_\alpha(\eta_{n+1}) = Y(\eta_n) + \alpha (Y(\eta_{n+1}) - Y(\eta_n)) = Y_n + \alpha \Delta Y \quad (\text{B.1})$$

$$Y(\eta_{n+\alpha}) \simeq Y_\alpha(\eta_{n+1}) = Y_n + \frac{\Delta Y^2}{\Delta Y + \frac{\partial Y(\eta_{n+1})}{\partial \eta_{n+1}} \Delta \eta} \quad (\text{B.2})$$

$$\begin{aligned}
 r(\eta_{n+1}) &= \frac{\partial \tilde{\Psi}_f^D}{\partial \eta_{n+1}} = -\varphi_f(\lambda_{f_{n+1}}) + \Delta t \frac{\partial \chi_f(\eta_{n+1})}{\partial \eta_{n+1}} \\
 &= -\varphi_f(\lambda_{f_{n+1}}) + Y_\alpha + \frac{\partial Y_\alpha}{\partial \eta_{n+1}} \Delta \eta = 0
 \end{aligned} \tag{B.3}$$

$$\frac{\partial Y_\alpha}{\partial \eta_{n+1}} = 2 \frac{\Delta Y}{\Delta Y + \frac{\partial Y(\eta_{n+1})}{\partial \eta_{n+1}} \Delta \eta} \frac{\partial \Delta Y}{\partial \eta_{n+1}} - \frac{\Delta Y^2}{\left(\Delta Y + \frac{\partial Y(\eta_{n+1})}{\partial \eta_{n+1}} \Delta \eta\right)^2} \left(2 \frac{\partial Y(\eta_{n+1})}{\partial \eta_{n+1}} + \frac{\partial^2 Y(\eta_{n+1})}{\partial (\eta_{n+1})^2} \Delta \eta\right)$$

$$\begin{aligned}
 r(\eta_{n+1}) &= \frac{\partial \tilde{\Psi}_f^D}{\partial \eta_{n+1}} = -\varphi_f(\lambda_{f_{n+1}}) + \Delta t \frac{\partial \chi_f(\eta_{n+1})}{\partial \eta_{n+1}} \\
 &= -\varphi_f(\lambda_{f_{n+1}}) + Y_\alpha + \frac{\partial Y_\alpha}{\partial \eta_{n+1}} \Delta \eta = 0
 \end{aligned} \tag{B.4}$$

#### ACKNOWLEDGEMENTS

Eduardo Alberto Fancello and Jakson Manfredini Vassoler thank the Brazilian ‘Conselho Nacional de Desenvolvimento Científico e Tecnológico’ who provided financial support for this research. We also thank the development team of METAFOR (LTAS-MN<sup>2</sup>L – Université de Liège, Belgium) for the permission of use and modification of the code.

#### REFERENCES

1. Lanir Y. Constitutive equations for fibrous connective tissues. *Journal of biomechanics* 1983; **16**(1):1–12.
2. Fung YC. *Biomechanics, Mechanical Properties of Living Tissues* (2nd edn). Springer: New York, 1993.
3. Mullins L. Softening of rubber by deformation. *Rubber Chemistry and Technology* 1969; **42**(1):339–362.
4. Weiss JA, Maker BN, Govindjee S. Finite element implementation of incompressible, transversely isotropic hyperelasticity. *Computer Methods in Applied Mechanics and Engineering* 1996; **135**(1-2):107–128.
5. Spencer AJM. *Continuum Theory of the Mechanics of Fibre-reinforced Composites*. Springer-Verlag: New York, 1984.
6. Balzani D, Neff P, Schröder J, Holzapfel G. A polyconvex framework for soft biological tissues. Adjustment to experimental data. *International Journal of Solids and Structures* 2006; **43**(20):6052–6070.
7. Balzani D, Schröder J, Gross D. Simulation of discontinuous damage incorporating residual stresses in circumferentially overstretched atherosclerotic arteries. *Acta Biomaterialia* 2006; **2**(6):609–18.
8. Simo JC. On a fully three dimensional finite-strain viscoelastic damage model: formulation and computational aspects. *Computer Methods in Applied Mechanics and Engineering* 1987; **60**:153–173.
9. Govindjee S, Simo JC. Mullins’s effect and the strain amplitude dependence of the storage modulus. *International Journal of Solids and Structures* 1992; **29**(14-15):1737–1751.
10. Peña E, Calvo B, Martínez M, Doblaré M. An anisotropic visco-hyperelastic model for ligaments at finite strains. Formulation and computational aspects. *International Journal of Solids and Structures* 2007; **44**(3-4):760–778.
11. Holzapfel GA, Gasser TC. A viscoelastic model for fiber-reinforced composites at finite strains: continuum basis, computational aspects and applications. *Computer Methods in Applied Mechanics and Engineering* 2001; **190**:4379–4403.
12. Peña E, Peña JA, Doblaré M. On modelling nonlinear viscoelastic effects in ligaments. *Journal of Biomechanics* 2008; **41**(12):2659–66.
13. Dorfmann A, Ogden R. A pseudo-elastic model for loading, partial unloading and reloading of particle-reinforced rubber. *International Journal of Solids and Structures* 2003; **40**(11):2699–2714.
14. Dorfmann A, Ogden R. A constitutive model for the Mullins effect with permanent set in particle-reinforced rubber. *International Journal of Solids and Structures* 2004; **41**(7):1855–1878.
15. Balzani D, Schroder J, Gross D. A simple model for anisotropic damage with applications to soft tissues. *Proceedings in Applied Mathematics and Mechanics* 2004; **237**:236–237.
16. Calvo B, Peña E, Martínez MA, Doblaré M. An uncoupled directional damage model for fibred biological soft tissues. Formulation and computational aspects. *International Journal for Numerical Methods in Engineering* 2007; **69**(10):2036–2057.
17. Peña E, Calvo B, Martínez M, Doblaré M. On finite-strain damage of viscoelastic-fibred materials. Application to soft biological tissues. *International Journal for Numerical Methods in Engineering* 2008; **74**(7):1198–1218.
18. Peña E. Damage functions of the internal variables for soft biological fibred tissues. *Mechanics Research Communications* 2011; **38**(8):610–615.

19. Rodríguez JF, Cacho F, Bea J, Doblaré M. A stochastic-structurally based three dimensional finite-strain damage model for fibrous soft tissue. *Journal of the Mechanics and Physics of Solids* 2006; **54**(4):864–886.
20. Rodríguez JF, Alastrue V, Doblaré M. Finite element implementation of a stochastic three dimensional finite-strain damage model for fibrous soft tissue. *Computer Methods in Applied Mechanics and Engineering* 2008; **197**(9-12):946–958.
21. Ehret AE, Itskov M. Modeling of anisotropic softening phenomena: application to soft biological tissues. *International Journal of Plasticity* 2009; **25**(5):901–919.
22. Christian Gasser T. An irreversible constitutive model for fibrous soft biological tissue: a 3-D microfiber approach with demonstrative application to abdominal aortic aneurysms. *Acta Biomaterialia* 2011; **7**(6):2457–66.
23. Peña E, Martins P, Mascarenhas T, Natal Jorge R, Ferreira A, Doblaré M, Calvo B. Mechanical characterization of the softening behavior of human vaginal tissue. *Journal of the Mechanical Behavior of Biomedical Materials* 2011; **4**(3):275–83.
24. Rickaby S, Scott N. A cyclic stress softening model for the Mullins effect. *International Journal of Solids and Structures* 2013; **50**(1):111–120.
25. Ortiz M, Stainier L. The variational formulation of viscoplastic constitutive updates. *Computer Methods in Applied Mechanics and Engineering* 1999; **171**:419–444.
26. Radovitzky R, Ortiz M. Error estimation and adaptive meshing in strongly nonlinear dynamic problems. *Computer Methods in Applied Mechanics and Engineering* 1999; **172**(1-4):203–240.
27. Fancello EA, Ponthot JP, Stainier L. A variational formulation of constitutive models and updates in non-linear finite viscoelasticity. *International Journal for Numerical Methods in Engineering* 2006; **65**(11):1831–1864.
28. El Sayed T, Mota A, Fraternali F, Ortiz M, Sayed El T, El T. A variational constitutive model for soft biological tissues. *Journal of Biomechanics* 2008; **41**(7):1458–1466.
29. Vassoler JM, Reips L, Fancello EA. A variational framework for fiber-reinforced viscoelastic soft tissues. *International Journal for Numerical Methods in Engineering* 2012; **89**(13):1691–1706.
30. Holzapfel GA. *Nonlinear Solid Mechanics: A Continuum Approach for Engineering*. Wiley: Chichester, 2000.
31. Sidoroff F. Un modèle viscoélastique non linéaire avec configuration intermédiaire. *Journal de Mécanique* 1974; **13**:679–713.
32. Le Tallec P, Kaiss A, Rahier C. Three-dimensional incompressible viscoelasticity in large strains: formulation and numerical approximation. *Computer Methods in Applied Mechanics and Engineering* 1993; **109**:223–258.
33. Reese S, Govindjee S. A theory for finite viscoelasticity and numerical aspects. *International Journal of Solids and Structures* 1998; **35**:3455–3482.
34. Fancello E, Vassoler JM, Stainier L. A variational constitutive update algorithm for a set of isotropic hyperelasticviscoplastic material models. *Computer Methods in Applied Mechanics and Engineering* 2008; **197**(49-50):4132–4148.
35. Sansour C. On the physical assumptions underlying the volumetric-isochoric split and the case of anisotropy. *European Journal of Mechanics - A/Solids* 2008; **27**(1):28–39.
36. Brassart L, Stainier L. On convergence properties of variational constitutive updates for elasto-visco-plasticity. *GAMM-Mitteilungen* 2012; **35**(1):26–42.
37. METAFOR. *METAFOR – Software for thermo-mechanical analysis of structures in large strain regime. Mécanique Numérique Non Linéaire*.
38. Muñoz MJ, Bea JA, Rodríguez JF, Ochoa I, Grasa J, Pérez del Palomar A, Zaragoza P, Osta R, Doblaré M. An experimental study of the mouse skin behaviour: damage and inelastic aspects. *Journal of Biomechanics* 2008; **41**(1): 93–99.